# Hercules-Aquila and Virgo Clouds with Gaia DR2. Evidence for a common origin

Keith T. Smith,[1]* A. N. Other,[2] Third Author[2,3] and Fourth Author[3]

[1]*Royal Astronomical Society, Burlington House, Piccadilly, London W1J 0BQ, UK*
[2]*Department, Institution, Street Address, City Postal Code, Country*
[3]*Another Department, Different Institution, Street Address, City Postal Code, Country*

## ABSTRACT

200 words for Letters. No references should appear in the abstract.

**Key words:** keyword1 – keyword2 – keyword3

## 1 INTRODUCTION

How do you hide the evidence for a massive impact event that caused the extinction of most of the dinosaurs as well as 75% of all species on Earth? You bury it deep under the sea, covered with a layer of sediment taller than the Empire State Building (Hildebrand et al. 1991). Without the discovery of the giant Chicxulub crater, the meteorite impact hypothesis would remain a neat theory supported by striking but indirect evidence. A hypothesis of an ancient dramatic collision between the Milky Way and an unidentified massive dwarf galaxy was put forward by Deason et al. (2013) to explain a particular feature in the overall stellar halo density profile (Watkins et al. 2009; Deason et al. 2011). Most recently, through a study of a portion of the nearby stellar halo, Belokurov et al. (2018b) demonstrated that the great impactor must have collided with the young Milky Way on a nearly radial orbit, thus swamping the inner stellar halo with metal-rich material with orbital anisotropy (see Binney & Tremaine 2008) close to unity. Merger events like this tend to leave behind a battery of debris clouds and shells (see Amorisco 2015; Hendel & Johnston 2015), which - akin to the peak rings of impact craters (see e.g. Morgan et al. 2016) - if discovered could help to reconstruct the collision as well as pin down the properties of the progenitor (e.g Sanderson & Helmi 2013; Johnston 2016).

Before the Data Release 2 (Gaia Collaboration et al. 2018) of the ESA's Gaia mission (Gaia Collaboration et al. 2016), five large and diffuse cloud-like structures had been discovered in the Galaxy's halo. These include: the Virgo Over-Density (VOD, Vivas et al. 2001; Newberg et al. 2002; Duffau et al. 2006; Jurić et al. 2008; Bonaca et al. 2012), the Hercules-Aquila Cloud (HAC, Belokurov et al. 2007; Simion et al. 2014), the Trinagulum-Andromeda structure (Tri-And, Rocha-Pinto et al. 2004; Majewski et al. 2004; Deason et al. 2014), the Pisces Over-density (Sesar et al. 2007; Watkins et al. 2009; Nie et al. 2015) and the Eridanus-Phoenix over-density (Eri-Pho, Li et al. 2016). According to the most recent investigations, Tri-And likely comprises of Galactic disc stars kicked out of the plane in a recent interaction with a dwarf galaxy, probably the

Sagittarius dSph (e.g. Price-Whelan et al. 2015; Bergemann et al. 2018; Hayes et al. 2018). Of the remaining four, the Pisces over-density clearly stands out as it reaches much larger Galacto-centric distances. On the other hand, the VOD, HAC and Eri-Pho structures occupy a very similar range of distances, between 10 and 20 kpc from the Galactic center. This lead Li et al. (2016) to suggest that these three Clouds could all be part of one merger event, a galaxy accreted onto the Milky Way on a polar orbit (see also Jurić et al. 2008).

As demonstrated by the recent re-interpretation of the Monoceros Ring (and the associated sub-structures) and the Tri-And, deciphering the nature of halo over-densities is often impossible without either high-resolution spectroscopy (e.g. Bergemann et al. 2018) or accurate astrometry (e.g. de Boer et al. 2018; Deason et al. 2018). In this Letter, we look for clues to the formation of the Hercules-Aquila and Virgo Clouds using proper motions provided as part of the Gaia DR2. At our disposal are highly pure samples of members of each Cloud, namely the RR Lyrae stars that i) are co-spatial with HAC and VOD in 3-D and ii) that have their line-of-sight velocities measured. By complementing the publicly available 4-D data with the GDR2 proper motions, we build a large tracer set with complete 6-D phase space information and study the make-up of each structure using the orbital properties of the constituent stars.

## 2 DATA AND ANALYSIS

Two samples of RR Lyrae with line-of-sight velocity measurements have been combined in this work to study the HAC and the VOD. Vivas et al. (2016) compiled a catalog of 412 RRL in the region of the VOD with distances between 4 and 75 kpc from the Sun. Simion et al. (2018) provides the radial velocities for 46 HAC RRL in a narrow distance range, between 15 and 18 kpc, where the peak of the HAC overdensity lies Simion et al. (2014).

---

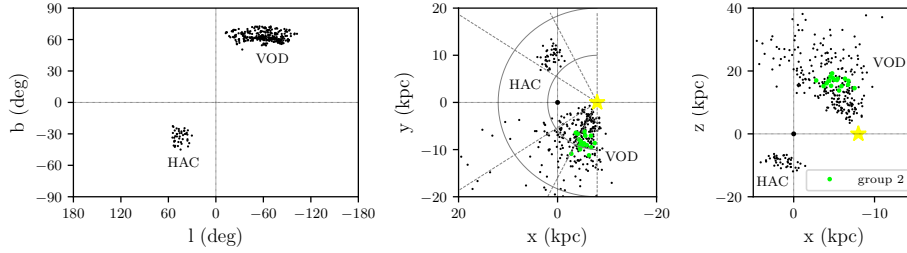* E-mail: mn@ras.org.uk (KTS)

**Figure 1.** Spatial distribution of the RR Lyrae used in this work with full 6-D phase space measurements, in Galactic coordinates (left panel) and in the $x - y$ (middle) and $y - z$ (right) planes. The HAC field contains 44 RR Lyrae which likely belong to the Cloud with measured line-of-sight velocities (Simion et al. 2018) and Gaia DR2 proper motions. The VOD field contains 411 RRL which belong to several halo associations, including the Sagittarius stream and the VOD, with line-of-sight velocities provided by Vivas et al. 2016 and proper motions from Gaia DR2. In particular we mark group 2, a 'high significance' kinematical group, which contains 18 stars (green circles). The semi-circles are centred on the Sun's position and have radius of 10 and 20 kpc. The Sun (yellow star) is located at $(x_\odot, y_\odot, z_\odot) = (0,-8,0)$ kpc and the Galactic centre at $(0,0,0)$ - black circle.

## 2.1   6-D Phase space measurements

44 of the 46 stars in table 1 in Simion et al. (2018) and 411 of the 412 in table 4 in Vivas et al. (2016) with matches within 2" in the Gaia DR2 catalog, have proper motion measurements.

The only star in the VOD region without proper motion measurement, belongs to a 'high-significance' kinematical group (group 1), likely the Sagittarius stream, identified by Vivas et al. (2016). 113 stars (112 with proper motions) belong to this group and we have excluded them for the analysis as a major contaminant of the VOD field. The spatial distribution of the remaining stars (44 from Simion et al. 2018 and 299 from Vivas et al. 2016) with full 6-D phase space measurements is illustrated in Figure 1, in Galactic coordinates (left panel) and in the Galactic plane and perpendicular to the Galactic plane projections. We adopted left-handed Galactic Cartesian coordinates with the Sun located at $(x_\odot, y_\odot, z_\odot) = (-8,0,0)$ kpc, the X-axis positive in the direction of the Galactic center, Y-axis oriented along the Galactic rotation and the Z-axis directed towards the north Galactic pole.

Vivas et al. 2016 identified 6 significant kinematical groups in the VOD field (their table 5) but only groups 1 and 2 (likely members of the VOD, with $< v_{GSR} > = 135$ km/s) contain more than 10 stars. We mark group 2 with green circles.

## 2.2   Velocity distribution

The velocity distribution in spherical polar coordinates ($v_r$, $v_\theta$, $v_\phi$ are the radial, azimuthal and polar components respectively) are shown in Fig. 2. To estimate the error on each velocity component we resample the data 1000 times from a multivariate Gaussian distribution with mean the measurement {ra$^i$, dec$^i$, d$^i$, pmra$^i$, pmdec$^i$, $v_h^i$} and full covariance matrix which takes into account the covariances between ra, dec and proper motions, provided by Gaia DR2. We take the standard deviation of the resulting {$v_r$, $v_\theta$, $v_\phi$} distributions as the upper limit of the velocity uncertainties. These errors are reported for all stars in Fig. 2. *Here I need to comment on the error bars, why so big for VOD, eg. higher distance, pm error etc.*

The orbital anisotropy, is highly radial in the HAC field ($\beta = 0.91 \pm 0.03$) where the stars are most likely members of the Cloud and radial in the VOD field ($\beta = 0.74 \pm 0.04$) in which stars span a much wider range of distances. The anisotropy values are the median and standard deviation over 500 non parametric bootstrap resampling trials. Each trial was modelled with a velocity ellipsoid using the Extreme Deconvolution module implemented in astroML
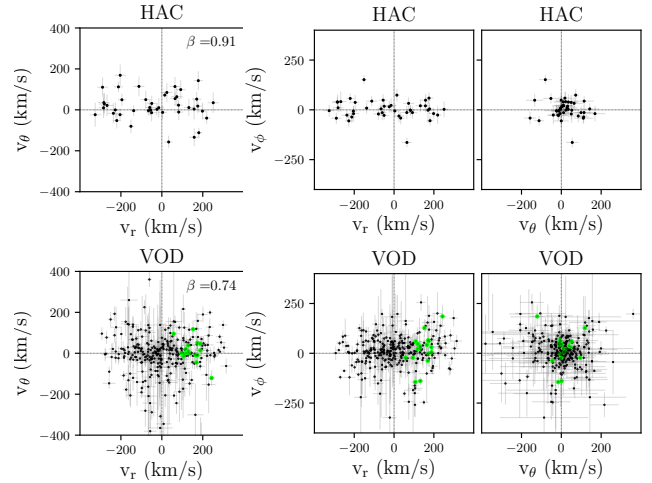


**Figure 2.** RRL velocity distribution in spherical polar coordinates ($v_r$, $v_\theta$, $v_\phi$ are the radial, azimuthal and polar components respectively) in the HAC field (top row) and the VOD field (middle and bottom rows). The error on the velocity components of each star $i$, [$\sigma_{v_r}^i$, $\sigma_{v_\theta}^i$, $\sigma_{v_\phi}^i$], has been propagated by randomly drawing 1000 stars from a multivariate Gaussian distribution with mean the measurement (ra$^i$, dec$^i$, d$^i$, pmra$^i$, pmdec$^i$, $v_h^i$) and full covariance matrix (takes into account the covariances between ra,dec and proper motions). The orbital anisotropy, is highly radial in the HAC field ($\beta = 0.91 \pm 0.03$) where the stars are most likely members of the Cloud and mildly radial in the VOD field ($\beta = 0.74 \pm 0.04$) in which stars span a much wider range of distances (see Fig. 1).
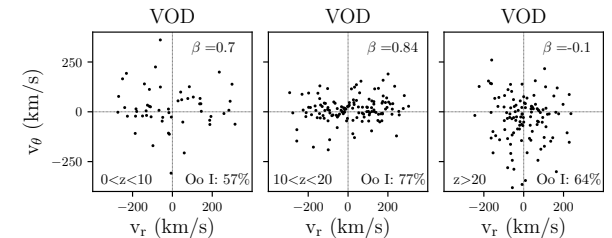


**Figure 3.** Radial versus azimuthal velocity in the VOD field, in three distance ranges above the Galactic plane. The fraction of RR Lyrae of Oosterhoff type I is reported in each panel.
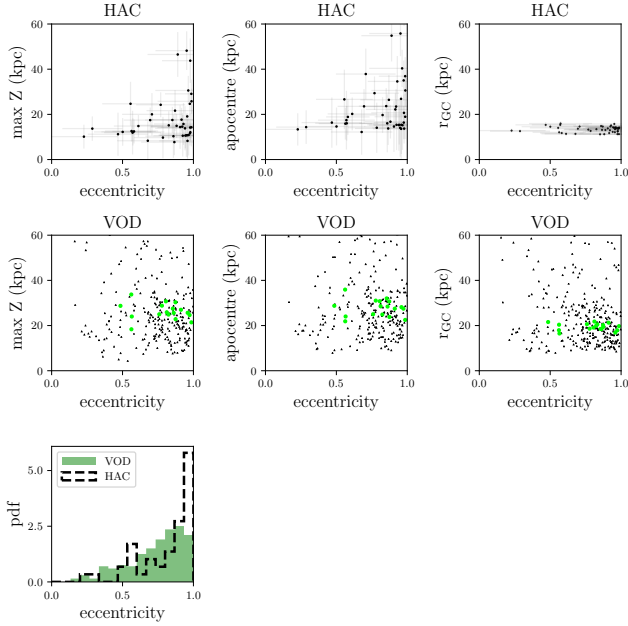
**Figure 4.** Orbital properties of the stars in the HAC and VOD fields. 'group 2' has similar orbital properties to the HAC, however it does not display a sausage velocity distribution (see middle row figure 2) - they are concentrated at $vr = 135$km/s as calculated by Vivas et al. 2016.

(Vanderplas et al. 2012).

Fig. 3 shows the behaviour of the VOD azimuthal $v_\theta$ and radial $v_r$ distributions in 3 distance slices above the Galactic plane. In each slice we have calculated the fraction of Oosterhoff type I (Oo I) RR Lyrae, using equations 1 and 2 in Belokurov et al. (2018a) to classify the RRL into two types. According to this classification, Oosterhoff type II (Oo II) RR Lyrae will incude both Oo II and Intermediate objects.

In the 10<z/kpc<20 range, where the orbital anisotropy is the highest ($\beta = 0.84 \pm 0.03$), the Oo I type dominates (77%), as in the HAC field (note: add number here). In the same slice, 73% of the stars belong to the 'sausage' component. The same behaviour but less accentuated can be noticed in the 0<z/kpc<10 slice where $\beta = 0.7 \pm 0.1$ is less radial but the fraction of Oo I stars decreases drammatically (note: comment if this is expected?). Further from the plane, at z>20 kpc, the velocity ellipsoid is almost isotropic with $\beta = -0.1 \pm 0.2$. We have excluded the most likely members of the Sagittarius stream but several others may remain, decreasing $\beta$.

## 2.3 Orbital properties of the HAC and VOD

We integrate orbits using the galpy package Bovy (2015) in the recommended MWPotential2014 model for the Galactic potential which is composed of a Miyamoto-Nagai disc, a bulge with a power-law density profile that is exponentially cut-off, and a dark matter halo described by a NFW potential. The parameters are given in table 1 Bovy (2015). The resulting orbital properties of the HAC and VOD are given in Fig 4. To compute the errors (not shown for VOD to simply the figure) we integrated 500 orbits for each star where the orbits were initialised on parameters resampled from data, as in the previous section. The pdf of the eccentricities is also shown.
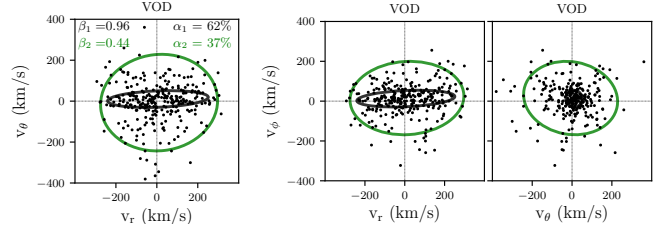
**Figure 5.** Result of the extreme deconvolution, $\beta_1 = 0.44^{+0.45}_{-0.20}$ and $\beta_2 = 0.96^{+0.02}_{-0.44}$.

## 3 DISCUSSION

### 3.1 ED of the VOD field

We model the VOD velocity ellipsoid with two multivariate Gaussians using extreme deconvolution. The result is shown in Fig. 5.

### 3.2 Are the VOD and HAC related?

Backward orbit integration. Talk about Figure 7.

## 4 CONCLUSIONS

## ACKNOWLEDGEMENTS

## REFERENCES

Amorisco N. C., 2015, MNRAS, 450, 575
Belokurov V., Deason A. J., Koposov S. E., Catelan M., Erkal D., Drake A. J., Evans N. W., 2018a, MNRAS, 477, 1472
Belokurov V., Erkal D., Evans N. W., Koposov S. E., Deason A. J., 2018b, MNRAS, 478, 611
Belokurov V., Evans N. W., Bell E. F., Irwin M. J. et al., 2007, ApJ, 657, L89
Bergemann M., Sesar B., Cohen J. G., Serenelli A. M. et al., 2018, Nature, 555, 334
Binney J., Tremaine S., 2008, Galactic Dynamics: Second Edition. Princeton University Press
Bonaca A., Jurić M., Ivezić Ž., Bizyaev D. et al., 2012, AJ, 143, 105
Bovy J., 2015, ApJS, 216, 29
de Boer T. J. L., Belokurov V., Koposov S. E., 2018, MNRAS, 473, 647
Deason A. J., Belokurov V., Evans N. W., 2011, MNRAS, 416, 2903
Deason A. J., Belokurov V., Evans N. W., Johnston K. V., 2013, ApJ, 763, 113
Deason A. J., Belokurov V., Hamren K. M., Koposov S. E. et al., 2014, MNRAS, 444, 3975
Deason A. J., Belokurov V., Koposov S. E., 2018, MNRAS, 473, 2428
Duffau S., Zinn R., Vivas A. K., Carraro G., Méndez R. A., Winnick R., Gallart C., 2006, ApJ, 636, L97
Gaia Collaboration, Brown A. G. A., Vallenari A., Prusti T., de Bruijne J. H. J., Babusiaux C., Bailer-Jones C. A. L., 2018, ArXiv e-prints
Gaia Collaboration, Prusti T., de Bruijne J. H. J., Brown A. G. A. et al., 2016, A&A, 595, A1
Hayes C. R., Majewski S. R., Hasselquist S., Beaton R. L. et al., 2018, ApJ, 859, L8
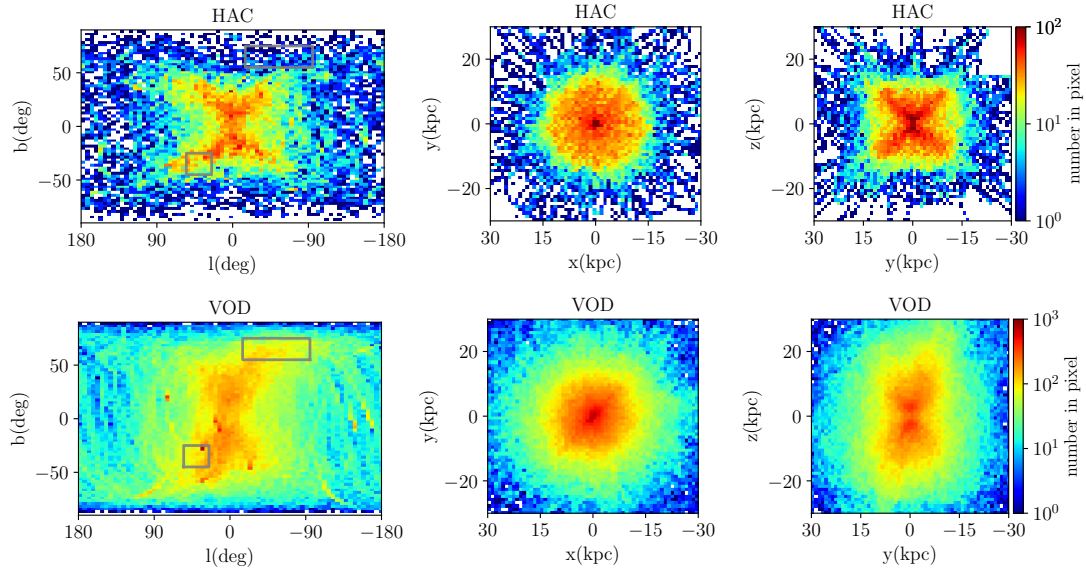Hendel D., Johnston K. V., 2015, MNRAS, 454, 2472

**Figure 6.** The backward orbit integration for HAC (top panels) and VOD (bottom panels) for 8 Gyrs look back time. We use $M_{vir} = 0.8 \times 10^{12} M_{\odot}$, the default galpy value . log(N) shown, notice the change in colour scale between top and bottom rows. The present day loci of HAC and VOD are marked with gray rectangles. The initial conditions of 44 stars with heliocentric distances between 15 and 18 kpc were used for the HAC backward orbit integration and of 299 stars with heliocentric distances between 4 and 75 kpc for the VOD orbit integration.
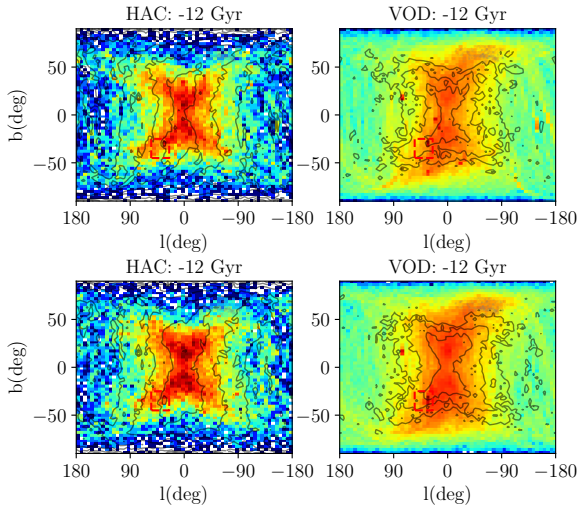


**Figure 7.** EXTRA: Look back time 12 Gyrs (8 Gyrs in Fig. 6). Here for the two sets of plots I have used different mass: top row $M_{vir} = 0.8 \times 10^{12} M_{\odot}$, bottom row $M_{vir} = 1.6 \times 10^{12} M_{\odot}$. HAC plots have VOD isodensity contours and viceversa.

Hildebrand A. R., Penfield G. T., Kring D. A., Pilkington M., Camargo Z. A., Jacobsen S. B., Boynton W. V., 1991, Geology, 19, 867

Johnston K. V., 2016, in Astrophysics and Space Science Library, Vol. 420, Tidal Streams in the Local Group and Beyond, Newberg H. J., Carlin J. L., eds., p. 141

Jurić M., Ivezić Ž., Brooks A., Lupton R. H. et al., 2008, ApJ, 673, 864

Li T. S., Balbinot E., Mondrik N., Marshall J. L. et al., 2016, ApJ, 817, 135

Majewski S. R., Ostheimer J. C., Rocha-Pinto H. J., Patterson R. J., Guhathakurta P., Reitzel D., 2004, ApJ, 615, 738

Morgan J. V., Gulick S. P. S., Bralower T., Chenot E. et al., 2016, Science, 354, 878

Newberg H. J., Yanny B., Rockosi C., Grebel E. K. et al., 2002, ApJ, 569, 245

Nie J. D., Smith M. C., Belokurov V., Fan X. H. et al., 2015, ApJ, 810, 153

Price-Whelan A. M., Johnston K. V., Sheffield A. A., Laporte C. F. P., Sesar B., 2015, MNRAS, 452, 676

Rocha-Pinto H. J., Majewski S. R., Skrutskie M. F., Crane J. D., Patterson R. J., 2004, ApJ, 615, 732

Sanderson R. E., Helmi A., 2013, MNRAS, 435, 378

Sesar B., Ivezić Ž., Lupton R. H., Jurić M. et al., 2007, AJ, 134, 2236

Simion I. T., Belokurov V., Irwin M., Koposov S. E., 2014, MNRAS, 440, 161

Simion I. T., Belokurov V., Koposov S. E., Sheffield A., Johnston K. V., 2018, MNRAS, 476, 3913

Vanderplas J., Connolly A., Ivezić Ž., Gray A., 2012, in Conference on Intelligent Data Understanding (CIDU), pp. 47 –54

Vivas A. K., Zinn R., Andrews P., Bailyn C. et al., 2001, ApJ, 554, L33

Vivas A. K., Zinn R., Farmer J., Duffau S., Ping Y., 2016, ApJ, 831, 165

Watkins L. L., Evans N. W., Belokurov V., Smith M. C. et al., 2009, MNRAS, 398, 1757

This paper has been typeset from a TEX/LATEX file prepared by the author.